AD-A181 576 VAPORIZATION IGNITION AND COMBUSTION OF TWO PARALLEL FUEL DROPLET STREAMS (U) CALIFORNIA UNIV IRVINE DEPT OF MECHANICAL ENGINEERING R H RANGEL ET AL MAR 87 1/1

UNCLASSIFIED AFOSR-TR-87-0592 AFOSR-86-0016 F/G 21/2 NL

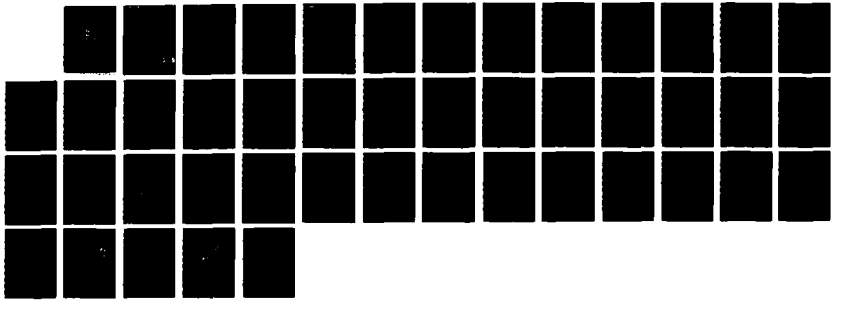

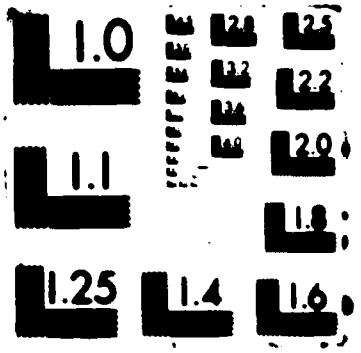
1.0
1.1
1.25
1.4
1.6
2.0
2.2
2.5

AFOSR-TR- 87-0592

(2)

Vaporization, Ignition, and Combustion of Two Parallel Fuel Droplet Streams

by

R.H. Rangel
and
W.A. Sirignano

Department of Mechanical Engineering
University of Califorina
Irvine, CA 92717

To be presented at the
2nd ASME-JSME
Thermal Engineering Joint Conference

Honolulu, Hawaii
March 22-27, 1987

ABSTRACT

An analysis of the combined mechanisms of heat transfer, vaporization, ignition, and combustion of two parallel fuel droplet streams injected in a hot, oxidizing gas flow is presented. The analysis gives a qualitative understanding of the various complex phenomena involved in the vaporization and ignition of one stream of droplets followed by the propagation of the flame to a second stream and the establishment of diffusion flames surrounding each droplet stream. The two-dimensional physical model consists of a constant-property oxidizing gas flowing with a uniform velocity between two insulated planes. The temperature of the gas at the inlet of the channel is specified. The fuel droplet streams are represented as two parallel droplet sheets injected at prescribed locations within the gas flow. Liquid temperature, droplet radius, as well as droplet-sheet density and velocity are specified at the inlet. By making some simplifications related to the fluid mechanics of the flow, a set of partial differential equations with linear operators and non-linear source terms governing the gas phase is found. The liquid phase is governed by a set of non-linear first-order ordinary differential equations. The gas-phase equations are solved with the aid of the Green's function technique, and the resulting integro-differential equations are numerically integrated together with the liquid-phase equations.

Results are presented for three different stream arrangements as well as for two different fuel types and two different inlet droplet radii. For the various cases considered, comparisons are made in terms of droplet vaporization distances, droplet lifetimes, ignition delays, and flame propagation rates. Droplet lifetimes and ignition delays are shown to decrease as fuel volatility increases and as inlet droplet size and lateral stream spacing decrease.

Unclassified
SECURITY CLASSIFICATION OF THIS PAGE

A181576

REPORT DOCUMENTATION PAGE

1a. REPORT SECURITY CLASSIFICATION Unclassified	1b. RESTRICTIVE MARKINGS None
2a. SECURITY CLASSIFICATION AUTHORITY Unclassified	3. DISTRIBUTION/AVAILABILITY OF REPORT Distribution unlimited; approved for public release
2b. DECLASSIFICATION/DOWNGRADING SCHEDULE Unclassified	
4. PERFORMING ORGANIZATION REPORT NUMBER(S)	5. MONITORING ORGANIZATION REPORT NUMBER(S) AFOSR-TR- 87-0592
6a. NAME OF PERFORMING ORGANIZATION University of California Dept. of Mechanical Engr.	6b. OFFICE SYMBOL (If applicable)
7a. NAME OF MONITORING ORGANIZATION Air Force Office of Scientific Research	
6c. ADDRESS (City, State and ZIP Code) Irvine, CA 92717	7b. ADDRESS (City, State and ZIP Code) BKG 410 Bolling AFB DC 20332-6448
8a. NAME OF FUNDING/SPONSORING ORGANIZATION Air Force Office of Sci. Res.	8b. OFFICE SYMBOL (If applicable) AFOSR/NA
9. PROCUREMENT INSTRUMENT IDENTIFICATION NUMBER AFOSR 86-0016	
8c. ADDRESS (City, State and ZIP Code) BKG 410 Bolling AFB DC 20332-6448	10. SOURCE OF FUNDING NOS. PROGRAM ELEMENT NO.: 61102F PROJECT NO.: 2308 TASK NO.: A2 WORK UNIT NO.:
11. TITLE (Include Security Classification) Vaporization, Ignition, and Combustion of Two Parallel Fuel Droplet Streams	
12. PERSONAL AUTHOR(S) R.H. Rangel and W.A. Sirignano	
13a. TYPE OF REPORT Publication	13b. TIME COVERED FROM 10/85 TO 10/86
14. DATE OF REPORT (Yr., Mo., Day) 3/87	15. PAGE COUNT 22
16. SUPPLEMENTARY NOTATION	

17. COSATI CODES		
FIELD	GROUP	SUB. GR

18. SUBJECT TERMS (Continue on reverse if necessary and identify by block number)
Spray Combustion; Iginition of Sprays; Flame Propagation in Sprays

19. ABSTRACT (Continue on reverse if necessary and identify by block number)

An analysis of the combined mechanisms of heat transfer, vaporization, ignition, and combustion of two parallel fuel droplet streams injected in a hot, oxidizing gas flow is presented. The analysis gives a qualitative understanding of the various complex phenomena involved in the vaporization and ignition of one stream of droplets followed by the propagation of the flame to a second stream and the establishment of diffusion flames surrounding each droplet stream. The two-dimensional physical model consists of a constant-property oxidizing gas flowing with a uniform velocity between two insulated planes. The temperature of the gas at the inlet of the channel is specified. The fuel droplet streams are represented as two parallel droplet sheets injected at prescribed locations within the gas flow. Liquid temperature, droplet radius, as well as droplet-sheet density and velocity are specified at the inlet. By making some simplifications related to the fluid mechanics of the flow, a set of partial differential equations with

20. DISTRIBUTION/AVAILABILITY OF ABSTRACT UNCLASSIFIED/UNLIMITED ☒ SAME AS RPT ☐ DTIC USERS ☐	21 ABSTRACT SECURITY CLASSIFICATION Unclassified
22a. NAME OF RESPONSIBLE INDIVIDUAL Julian M. Tishkoff	22b TELEPHONE NUMBER (Include Area Code) (202) 767-4935
	22c OFFICE SYMBOL AFOSR/NA

DD FORM 1473, 83 APR EDITION OF 1 JAN 73 IS OBSOLETE

Unclassified
SECURITY CLASSIFICATION OF THIS PAGE

87 5 21 [illegible] 5

linear operators and non-linear source terms governing the gas phase is found. The liquid phase is governed by a set of non-linear first-order ordinary differential equations. The gas-phase equations are solved with the aid of the Greens' function technique, and the resulting integro-differential equations are numerically integrated together with the liquid-phase equations.

Results are presented for three different stream arrangements as well as for two different fuel types and two different inlet droplet radii. For the various cases considered, comparisons are made in terms of droplet vaporization distances, droplet lifetimes, ignition delays, and flame propagation rates. Droplet lifetimes and ignition delays are shown to decrease as fuel volatility increases and as inlet droplet size and lateral stream spacing decrease.

NOMENCLATURE

A	preexponential factor
A_n	numeric coefficient, $A_n = 1$ for $n = 0$, $A_n = 2$ for $n \geq 1$
B	transfer number, $B = \frac{C_p(T-T_\ell)}{L_v}$
B_{eff}	effective transfer number, $B_{eff} = \frac{C_p(T-T_\ell)}{L_{eff}} = \frac{Y_{Fs} - Y_F}{1 - Y_{Fs}}$
C_d	drag coefficient, $C_d = (24/Re)(1 + Re^{2/3}/6)$
C_ℓ	liquid-phase specific heat
C_p	gas-phase specific heat at constant pressure
D	gas diffusivity
G	Green's function, $G = G(\xi,\chi\|\xi',\chi')$
I_{cn}	combustion integral (eq. 8)
j	summation index referring to droplet streams
J_k	dimensionless gas-phase variables
L	channel width
L_v	latent heat of vaporization of fuel
m	droplet mass
$\dot{m}$	droplet vaporization rate, $\dot{m} = 4\pi R\rho D\,(1 + 0.3\,Re^{0.5})\,\ell n\,(1 + B_{eff})$
M	molecular weight
N	number of droplet streams
N_ℓ	droplet-sheet density
P_1	vaporization/diffusion length ratio, $P_1 = (R_i^2\rho_\ell U_\ell)/(3L^2\rho U_g)$
P_2	fuel/air mass flow ratio, $P_2 = (N_{\ell i} m_i U_{\ell i})/(L\rho U_g)$
P_5	vaporization/reaction length ratio, $P_5 = (R_i^2\rho_\ell U_{\ell i} A\, M_F^{1-a})/(3DU_g M_O^{b}\rho^{2-a-b})$
P_7	oxygen/fuel stoichiometric mass ratio, $P_7 = \frac{\nu_O M_O}{M_F}$

Q heat of combustion

R droplet radius

Re Reynolds number, $Re = (2R|U_g - U_\ell|)/\nu$

S_c combustion source, $S_c = Y_F^a Y_O^b \exp(-E/R^0 T)$

S_v dimensionless vaporization rate, $S_v = \dot{m}/(4\pi R_i \rho D)$

S_{v1} vaporization source in fuel equation, $S_{v1} = (1 - Y_F) N'_\ell S_v$

S_{v2} vaporization source in oxygen equation, $S_{v2} = -P_7^{-1} Y_O N'_\ell S_v$

S_{v3} vaporization source in gas-phase energy equation,

$$S_{v3} = -P_6(1 + B_{eff}^{-1})(T' - T'_\ell)N'_\ell S_v$$

T temperature

T' dimensionless temperature, $T' = \dfrac{T - T_{\ell i}}{T_r - T_{\ell i}}$

U velocity

x transverse coordinate

Y mass fraction

z streamwise coordinate

Greek Symbols

γ_n parameter, $\gamma_n = P_1 n^2 \pi^2$

δ' dimensionless delta function

ν kinematic viscosity

ν_o oxygen/fuel stoichiometric molar ratio

ξ dimensionless streamwise coordinate, $\xi = z/(R_i^2 \rho_\ell U_{\ell i}/3\rho D)$

ρ gas density

χ dimensionless transverse coordinate, $\chi = x/L$

Subscripts

F	fuel
g	gas
i	inlet
j	stream number, j = 1, ..., N
k	denotes k-th gas-phase independent variable, k = 1, 2, 3
ℓ	liquid
n	denotes n-th component of series
O	oxygen
r	reference
s	droplet surface

INTRODUCTION

The analytical study of fuel spray combustion is of interest in the design and emission control of diesel, turbine, and jet engines. Mathematical and numerical models of realistic spray combustion situations are highly complicated by the probabilistic character of the initial conditions, the amount of nonlinearities present in the governing equations and the very strong coupling existing between the gas and liquid phases. Evidence of these complexities is manifest even in the vaporization studies of isolated droplets [1]-[3], and in those considering a group of interacting liquid droplets [4]-[6].

More involved investigations of multidimensional sprays must take into account a large number of droplets, consequently requiring a large number of equations and large amounts of computational time. From the numerical point of view, accurate representation of ignition and flame propagation in sprays requires resolution on a scale which is smaller than the typical droplet spacing. The reason for this is that the thickness of typical reation zones is of the order of the droplet spacing. The existence of individual or group flames, the rate of propagation of the chemical reaction, and the droplet lifetimes are all intimately linked to the particular space and size distributions of the spray. Since these distributions are the result of the highly non-linear and poorly understood atomization process, they are generally known only in a statistical fashion, therefore imposing severe limitations to a deterministic spray combustion model. It should be emphasized, however, that if the initial spray conditions are specified, deterministic methods can be employed to describe the spray behavior. Finite-difference methods have been used to solve one-dimensional, unsteady spray combustion problems using a gas-phase discretization which permits resolution

on the scale of the distance between droplets [7]-[9].

An extension of the one-dimensional models just described to multi-dimensional situations implies a very large increase in computational time and an increasing number of influencing parameters. It is advantageous to initiate the study of two- and three-dimensional spray situations with a simplified model more amenable to analytical treatment but still retaining most of the interesting physics. In our basic model of spray combustion, a configuration consisting of multiple parallel droplet streams injected in an air flow is considered. Experimental and theoretical studies of single streams of monosized droplets have been reported in the literature [9]-[10]. The mathematical model employed in those calculations made use of the Green's function technique to consider the limits of an isolated droplet and a cylindrical filament. Experimental work with multiple parallel streams has also been initiated [11] and will serve as a point of comparison for the analytical model proposed here once this is refined by relaxing some simplifying assumptions. In a previous work [12], we have reported a parametric study of a two-stream non-reactive spray system using the Green's function approach to solve the gas-phase equations. In this work, a one step chemical reaction rate [13] is included in the model in order to explore the flame behavior for a variety of spray configurations. By simplifying the fluid mechanics of the flow one is able to concentrate on the non-linear heat and mass transfer interactions of the gas and liquid phases as well as on the complexities of the flame propagation mechanism, and to understand their dependence on stream spacing and other spray properties. The model thus represents a sound first approach to more realistic situations in which the spray properties (droplet size and space distributions) possess a more chaotic character. It is expected that future improvements of the analysis

presented here will permit the study of fluctuating inlet conditions and more arbitrary droplet distributions.

ANALYSIS

a) Description of the Problem

Figure 1 shows a schematic of the problem under consideration. A constant property gas is flowing with a uniform velocity U_g in a channel of width L bounded by two insulated parallel planes. In this figure, the channel inlet is located at the bottom and the flow direction is upward. The flow is two-dimensional and steady, and viscosity is neglected except in the calculation of droplet drag. The uniform flow velocity represents a first approach to the real description of the fluid mechanics of the problem. Gas expansion resulting from heating can be easily incorporated into the model at some future point. Two parallel droplet streams are injected with the same velocity $U_{\ell i}$ at the inlet of the channel and at specified transverse locations. The droplets always maintain their initial flow direction parallel to the boundary planes but they experience acceleration or deceleration due to viscous drag. Gas and droplet temperature and velocity as well as droplet radius are specified at the channel inlet. The gas temperature at the channel inlet is prescribed as a linear profile with the highest temperature point located at the left wall. As the droplets heat up and vaporize in the hot gas, the concentration of fuel vapor in the gas phase increases. Then, at some point downstream, a chemical reaction is initiated which propagates throughout the channel in a manner to be investigated. A one step chemical reaction of the Arrhenius type is assumed.

b) Liquid-Phase Equations

The droplets are assumed to remain spherical at all times and an infinite conductivity model is adopted. Accordingly, no spatial temperature gradients exist inside the droplets. More accurate models of droplet heating and vaporization such as that of references [14] and [15] can be incorporated without difficulty. The spherically symmetric vaporization model of reference [16] is employed with no envelope flames considered and with a correction term to account for convective effects. The dimensionless equations for conservation of droplet number, mass, energy and momentum for an individual droplet in a stream are:

$$\frac{d}{d\xi}\,(U_\ell' N_\ell) = 0 \tag{1a}$$

$$U_\ell' \frac{dR'^3}{d\xi} = -S_v \tag{1b}$$

$$R'^3\, U_\ell' \frac{dT_\ell'}{d\xi} = C_p\,(T' - T_\ell')(B_{eff}^{-1} - B^{-1})\, S_v/C_\ell \tag{1c}$$

$$U_\ell' \frac{dU_\ell'}{d\xi} = (C_d/16)\, Re(U_g' - U_\ell')/R'^2 \tag{1d}$$

where the various symbols as well as the choice of dimensionless variables are given in the nomenclature. We note that B_{eff} is an effective transfer number that takes into account the transient heating of the droplet, while B is the standard transfer number. Primes are used to indicate dimensionless quantities. At the channel inlet we specify the values of the liquid velocity, the liquid temperature, the droplet radius, and the droplet-sheet density. In dimensionless form these conditions are: $U_\ell' = 1$, $T_\ell' = 0$, $R' = 1$, and $N_\ell' = 1$ at $\xi = 0$.

In addition to eqs. (1a)-(1d) there is a Clasius-Clapeyron equilibrium equation relating the fuel vapor concentration at the droplet surface Y_{F_S} to the droplet temperature.

c) Gas-Phase Equations

A number of assumptions are made in order to reduce the problem to a set of equations amenable to analytical solution. By assuming constant physical properties and uniform pressure, and neglecting the mass contribution from the vaporization process, the equations of conservation of mass and momentum are rendered trivial and yield the uniform gas velocity U_g. As mentioned earlier, the acceleration of the flow due to thermal expansion will be incorporated in the future. In the case of an overall equivalence ratio of one, the additional mass produced by the vaporization process amounts to approximately 7% of the total mass flow. Therefore, it is reasonable to neglect it within the margin of other assumptions invoked in this model. Also neglected are the convective terms in the transverse direction as well as heat and species diffusion in the axial direction. This latter assumption is expected to be appropriate for gas Peclet numbers larger than 10 except in the vicinity of regions with large temperature or species-concentration gradients. If the droplets within a stream are not very far from each other or if we want to be concerned with some type of time-averaged representation of the vaporization and combustion processes, we may assume that, from the gas-phase point of view, the droplets within a stream represent spatially continuous sources of fuel vapor and sinks of energy. Within the context of our two-dimensional model, the droplets are then contained in planar droplet sheets which are parallel to the channel walls. The droplet density on these sheets is specified at the inlet but it varies with downstream distance as the droplets

accelerate or decelerate under the action of the drag force.

The dimensionless gas-phase equations governing the conservation of fuel, oxygen, and energy can be written in one compact form as:

$$\frac{\partial J_k}{\partial \xi} - P_1 \frac{\partial^2 J_k}{\partial \chi^2} = \sum_{j=1}^{N} P_2 \, S_{vk} \, \delta'(\chi - \chi_j) - P_5 S_c \qquad (2)$$

for k = 1, 2, 3. Here J_1, J_2, and J_3 stand respectively for Y_F, Y_O/P_7, and P_6T', where P_7 is the oxygen/fuel stoichiometric mass ratio and P_6 is a dimensionless parameter involving the heat of reaction. ξ and χ are the streamwise and tranverse coordinates respectively. The linear differential operator on the left hand side is composed of two terms which are respectively the convective term in the streamwise direction and the diffusion term in the transverse direction. The right hand side contains two types of source terms. The vaporization terms are contained in the summation sign where N is the number of streams. These terms are non-zero only at the location of the streams as evidenced by the delta functions $\delta'(\chi - \chi_j)$. The chemical reaction source is represented by the last term on equation (2) which contains a finite rate reaction of the Arrhenius type. Both the vaporization and chemical-reaction source terms are highly non-linear as may be seen from the expressions for the various S_{vk}'s and for S_c given in the nomenclature. The various parameters P_1 through P_7 are also given in the nomenclature. The boundary conditions to be satisfied by equation (2) are:

$$J_k = J_{ki} \text{ at } \xi = 0 \qquad (3a)$$

$$\frac{\partial J_k}{\partial \chi} = 0 \text{ at } \chi = 0 \text{ and } \chi = 1 \qquad (3b)$$

The first of these conditions refers to the specified values of fuel mass fraction, oxygen mass fraction, and temperature at the channel inlet, while the second condition indicates that there is no diffusion of species nor heat transfer at the side walls.

d) Method of Solution

The liquid phase is governed by a set of non-linear, coupled, ordinary differential equations which could be readily integrated with a numerical scheme if the solution of the gas-phase equations were known. The linearity of the differential operators in the gas-phase equations suggests the use of the Green's function technique in their solution. Reference [17] illustrates the use of Green's functions in mathematical problems. The solution of the three gas-phase equations represented by equation (2) will be obtained with the aid of the Green's function $G(\xi, \chi/\xi', \chi')$ satisfying the following equation and boundary conditions:

$$\frac{\partial G}{\partial \xi} - P_1 \frac{\partial^2 G}{\partial \chi^2} = \delta'(\xi - \xi')\,\delta'(\chi - \chi') \qquad (4)$$

$G = 0$ for $\xi < \xi'$, $\frac{\partial G}{\partial \chi} = 0$ at $\chi = 0$ and $\chi = 1$.

This Green's function corresponds to the temperature distribution in a slab subject to an instantaneous energy release at time $\xi = \xi'$ at the point $\chi = \chi'$. The solution of this problem is given in [18]. Solution of equations (2) can be obtained in terms of the Green's function G by combining equations (2) and (4) and integrating over the domain $0 \leq \chi' \leq 1$, $0 \leq \xi' \leq \xi$ in the manner described in [19]. The result is a set of non-linear integral equations which represent a closed form solution of the gas-phase equations:

$$J_k = \int_0^1 J_{k1} G|_{\xi'=0} d\chi' + \int_0^\xi \sum_{j=I}^{N} P_2 (S_{vk} G)|_{\chi'=\chi_j} d\xi' - \int_0^\xi \int_0^1 P_5 S_c G d\chi' d\xi' \tag{5}$$

These integral equations, however, cannot be readily evaluated because the integrands are functions of the gas and liquid independent variables. In order to numerically evaluate the solution, it is useful to note the series character of the Green's function [12], and write the solution as:

$$J_k(\xi, \chi) = \sum_{n=0}^{\infty} A_n \, J_{kn}(\xi) \cos(n\pi\chi) \tag{6}$$

Then, by differentiating the integral equations (5) with respect to ξ one obtains:

$$\frac{dJ_{kn}}{d\xi} = \sum_{j=I}^{N} (P_2 \, S_{vk} \cos(n\pi\chi'))|_{\chi'=\chi_j} - P_5 \, I_{cn} - \gamma_n J_{kn} \tag{7}$$

where:

$$I_{cn} = \int_0^1 Sc \cos(n\pi\chi') d\chi' \tag{8}$$

Equation (7) is an integro-differential equation (the integral occurring in the transverse direction as given by equation (8) and the first-order differential occurring in the streamwise direction) which is subject to the inlet condition:

$$J_{kn} = \int_0^1 J_{k1} \cos(n\pi\chi') d\chi' \tag{9}$$

The boundary conditions at the side walls are immediately satisfied by the series solution of equation (6). Equations (1a-d) and (7) are simultaneously

integrated in the streamwise direction. The number of terms (as given by n in equation (7)) required by the gas-phase solution is imposed by the specified accuracy desired and it lies between 15 and 20. A total of n numerical integrations as given by equation (8) must be performed at each axial step in order to evaluate the effects of the distributed chemical reaction. Typical CPU times in a VAX 11/750 are 5 minutes.

RESULTS AND DISCUSSION

a) Base-Case Calculation

The base-case calculation is for normal-decane fuel droplets with inlet diameters of 100 μm, inlet temperature of 300°K, and inlet velocity of 10 m/s. The droplet streams are injected in air flowing at a uniform velocity of 5 m/s. The pressure is 10 atm, the inlet oxygen mass fraction is 0.23, and the inlet fuel mass fraction is 0. The gas-phase inlet temperature profile is linear with a maximum of 1400°K at the left wall and a minimum of 400K at the right wall. The side walls are kept insulated downstream of the channel inlet. The overall equivalence ratio of the incoming air/fuel flow is 1.0. The channel width is 0.6 cm, and the droplet streams are located respectively at 0.2 cm and 0.4 cm from the left wall.

Figure 2 shows the development with downstream distance of the gas-phase temperature profile. At the inlet (ξ = 0) the gas-phase temperature profile is linear with a maximum on the left wall. Further downstream (ξ = 0.25) and due to heat diffusion in the transverse direction the left wall temperature and the right wall temperature respectively decrease and increase slightly. To the left of the first droplet stream a chemical reaction is initiated as indicated by the small temperature increase shown for ξ = 0.25 at χ = 0.25. The incipient chemical reaction has a lean premixed character and is the

result of the mixing of oxygen and fuel in the presence of an elevated gas temperature. As this premixed flame propagates to the right, the temperature increases, peaking first at the location of the left droplet stream (ξ = 0.5) and again as the flame reaches the right droplet stream (ξ = 0.75). Further downstream (ξ = 1.0), a relatively uniform high temperature profile results when almost all the fuel has been depleted and the gas-diffusion mechanism redistributes the energy across the channel.

The fuel vapor mass fraction is presented in Fig. 3, where the contour lines of constant fuel mass fraction are shown. Near the inlet of the channel no significant amounts of fuel vapor are produced because most of the heat transferred to the droplets is used to increase the liquid temperature. The fuel mass fraction reaches a first relative maximum at the location of the left droplet stream 16 cm from the channel inlet (dimensionless downstream distance of 0.32 in Fig. 3), and a second relative maximum at the location of the right stream 22 cm from the channel inlet (dimensionless downstream distance of 0.45). After reaching those maxima, the fuel vapors are depleted by the premixed flame which propagates from left to right. Since the droplets still exist beyond the location of the premixed flame, more fuel vapor is produced at the location of the droplet streams. These new fuel vapors diffuse away from the streams where the oxygen mass fraction has now been reduced to zero. The outwardly diffusing fuel meets the inwardly diffusing oxygen to produce the pattern of diffusion flames surrounding the droplet streams which is shown in Fig. 3.

The gas-phase oxygen mass fraction is presented in Fig. 4. At the channel inlet (ξ = 0) the oxygen mass fraction is 0.23 corresponding to the fresh incoming air flow. Oxygen is first consumed near the location of the left stream by the incipient premixed flame (ξ = 0.25). As this premixed

flame propagates towards the right, oxygen is further consumed along the flame front, particularly at the location of the droplet streams, where the chemical reaction is faster (curve for $\xi = 0.50$). The curves corresponding to $\xi = 0.75$ and $\xi = 1.0$ show that oxygen has been depleted in the center of the channel and is diffusing from the regions next to the side walls towards the weakening reaction zones which surround the second droplet stream. The first droplet stream has completely vaporized at $\xi = 0.6$.

Figures 5-8 show the dimensionless gas-phase reaction rate profiles at four different downstream locations. Figure 5 ($\xi = 0.32$) shows the initiation of a relatively thick reaction zone on the left side of the first droplet stream. This is the premixed flame resulting from the mixing of air and fuel during the initial droplet-vaporization period. In Figure 6 ($\xi = 0.49$) the premixed flame (seen as the thickest reaction zone on the right) has reached the location of the second droplet stream, while a thinner diffusion flame has been formed on each side of the first droplet stream. There is no oxygen present between the two diffusion flames and no fuel outside of them. Figure 7 ($\xi = 0.58$) shows that the premixed flame has almost reached the right wall and has become very weak due mainly to the lower initial gas temperature prevailing in this zone. Each droplet stream is now surrounded by two thin diffusion flames with the outer flames being somewhat stronger than the inner ones because of the steeper oxygen gradients existing on the outer side. The situation shown in Figure 8 ($\xi = 0.70$) indicates that oxygen has been depleted between the droplet streams and the innermost diffusion flames have consequently been extinguished. The two remaining diffusion flames are now surrounding the fuel vapors left in the center of the channel. These flames become weaker and are ultimately extinguished when the fuel vapors and the oxygen are depleted.

Figures 9-12 refer to the droplets within the streams. The left and right streams are denoted by I and II respectively. In Fig. 9 we see the transient behavior of the dimensionless liquid temperature. The droplets enter the channel at a temperature of 300°K (dimensionless temperature = 0.0) and undergo a transient heating process lasting approximately 75% of the droplet lifetime until they reach an equilibrium temperature of 498°K along the first stream and of 495°K along the second stream. These equilibrium temperatures are perceptibly lower than the saturation temperature of 537°K (dimensionless temperature = 0.215) corresponding to the prevailing pressure. The sudden increase observed in the heating rates occurs when the droplets cross the premixed flame and enter the region of high gas temperature. Figure 10 shows the dimensionless vaporization rate for each droplet stream. The vaporization rate is low first when the droplets are relatively cold. Then it increases as the droplet temperature increases, experiencing a sudden increase when the droplets cross the premixed flame. Later, as the droplet size decreases the vaporization rate gradually reduces to zero. The effective transfer number based on an effective heat of vaporization which accounts for the effect of droplet heating is shown in Figure 11. Initially the droplet temperature is low which results in a low fuel mass fraction at the surface and a low transfer number. As the droplet temperature increases, the transfer number increases slowly, and when the gas temperature increases as a result of the exothermic rection, the effective transfer number rises sharply until it reaches an almost constant value which is higher for the first stream due to the higher gas-temperature existing near it. The variation with downstream distance of the droplet radius squared is presented in Figure 12. After the initial heating period, the variation with downstream distance of the droplet radius squared is essentially linear.

Since the droplet velocity is decreasing, this indicates that the variation with time of the droplet radius squared is not linear which can be explained by the decreasing Reynolds number which appears in the convective correction to the vaporization rate S_v. The vaporization distance for the droplets on the first stream is 30 cm and for the droplets on the second stream this distance is 38 cm. The droplet lifetimes are 42 ms and 57 ms respectively.

b) Effect of Stream Arrangement

In order to look at the effect of different stream arrangements on ignition, flame propagation and droplet lifetimes, three stream arrangements are considered. In all cases the first stream is located at 1/3 of the channel transverse dimension while the second stream is located at 1/2 (case A), 2/3 (case B), and 5/6 (case C) of the transverse dimension respectively. We note that case B corresponds to the base-case calculation. All other parameters are the same as in the base case.

Figures 13 and 14 show the constant-fuel-mass-fraction contour lines for cases A and C respectively. The corresponding plot for case B is shown in Fig. 3 and was discussed in the previous section. Comparing cases A, B, and C one observes different flame behaviors related to different stream spacings. In case A (Fig. 13) the two streams are sufficiently close to inhibit the development of individual flames around each stream. Instead, both streams are surrounded by the same diffusion flame with no oxygen present between the streams beyond the location of the premixed flame. In case B (Fig. 3), individual stream flames develop which eventually merge when the oxygen between the streams is depleted. We note that for oxygen-rich sprays (overall equivalence ratios less than 1), the individual flames would persist without merging for a longer distance since there would be more oxygen available

between the streams. In case C (Fig. 14) the streams are sufficiently far apart to prevent the direct interaction between the diffusion flames which surround each stream. Therefore, an envelope flame is established on a segment of the first stream with fuel vapors inside the flame and oxygen outside of it.

Comparisons between the three stream arrangements have been made in terms of droplet vaporization distances, droplet lifetimes, ignition delays between the first and second streams, and flame propagation rates in the transverse direction. The results are contained in Table 1 where the aforementioned parameters are tabulated for the arrangements A, B, and C. Roman numerals I and II refer to the first and second stream respectively. Droplet vaporization distances for stream II are increased as this stream is positioned farther away from the first stream and therefore from the hot wall. The vaporization distance for stream I remains the same for cases B and C indicating that for these stream spacings no effect is felt by the first stream due to the presence of the second one. For case A, however, a slight increase in the vaporization distance is observed for stream I in comparison with cases B and C indicating that the presence of stream II is now manifest on stream I through a reduction in the amount of energy available per droplet to effect vaporization. The droplet lifetimes, which are the integrals along the streams of the quantity dz/U_ℓ from the inlet to the point of complete vaporization, show essentially the same behavior as the droplet vaporization distance. The ignition delay contained in Table 1 is defined as $\Delta z_{ig}/U_g$ where Δz_{ig} is the distance, in the downstream direction, at which the premixed flame reaches the second stream minus the corresponding distance for the first stream. As may be intuitively predicted, the ignition delay increases as the second stream is displaced towards the right wall away from the first stream

and the hot wall. Also included in Table 1 is the flame propagation rate in the transverse direction defined as the ratio between the transverse stream spacing and the ignition delay previously described. The flame propagation rate has a value of 34 cm/s for case A, decreases to 13 cm/s for case B, but shows almost no variation between cases B and C.

c) Effect of Droplet Size and Fuel Volatility

In order to establish the effect of inlet droplet size and fuel volatility on the combustion parameters of interest, two different droplet sizes and two different fuel types are considered. For the effects of this parametric study, the stream arrangement corresponds to that of the base case. The droplet diameters are 100 μm and 50 μm and the fuels are normal decane and normal hexane. The overall equivalence ratio is one for all cases and all other parameters are the same as in the base case previously discussed.

Figures 15 and 16 show the variation of the droplet-radius squared and the gas-phase fuel mass fraction contours for the case of 50 μm n-decane droplets. Note that the streamwise scale in these figures is different from that of the base case. While a dimensionless streamwise distance of 1.0 represented a real distance of 0.48 m in the base case, here the same dimensionless streamwise distance represents a real distance of 0.12 m. With the smaller droplets, the vaporization rate is larger which results in shorter vaporization distances and droplet lifetimes as can be seen in Table 2. Because a larger amount of fuel vapor is produced in the inlet region, the premixed flame is established closer to the channel inlet. With the 50 μm droplets, approximately 46% of the droplet mass is vaporized ahead of the flame along the first stream while with the 100 μm droplets this amount is

only 12%. This indicates that as the inlet droplet radius is decreased the spray more closely resembles the features of a premixed fuel. However, in order to fully approach the limit of a premixed fuel, the number of streams must be correspondingly increased. In our case, because the number of streams is kept at two while the droplet radius is decreased, the local equivalence ratio at the location of the fuel stream just ahead of the premixed flame is slightly larger than one (fuel rich). This results in the oxygen being locally depleted at the location of the premixed flame. The excess fuel mixes with the fuel vapors produced behind the premixed flame and burns in the diffusion flames subsequently established (Fig. 16). The delay in igniting the second stream is reduced and the transversal flame propagation rate is enhanced as indicated in Table 2.

Changing the fuel to normal-hexane produces the same effects in the droplet lifetimes and flame propagation rates as those described for smaller inlet droplets, although the variations are less pronounced. Column 3 of Table 2 contains the results for 100 μm droplets on n-hexane for an overall equivalence ratio of 1.0. Since n-hexane is more volatile than n-decane, fuel vaporization is faster with the former and shorter lifetimes and greater flame propagation rates result. The last column of Table 2 contains the results for 50 μm droplets of n-hexane. Here the added effects of a higher volatility and a larger total droplet surface area result in a very much enhanced flame propagation rate and a shorter ignition delay. In this case approximately 50% of the liquid is vaporized ahead of the reaction zone.

CONCLUSIONS

A two-dimensional model of a fuel spray consisting of parallel droplet streams injected in an air flow has been presented. By simplifying some

aspects of the flow dynamics of the problem, a gas-phase solution in the form of non-linear integral equations has been obtained. These gas-phase integral equations are further transformed to a set of integro-differential equations which are numerically integrated together with the liquid-phase equations. Since the fuel streams are considered to be discrete identities in the traverse direction, spacial resolution on the scale of the stream spacing is possible which permits the study of the influence of stream separation on ignition delays and flame propagation rates. Within the range of parameters considered in this study, the reactive flow is characterized by an inlet pre-ignition zone followed by a premixed flame which acts as the ignition source of the fuel streams. Further downstream, a pattern of diffusion flames surrounding individual streams or a group of them is established. The model may be extended to include the characteristic unsteadiness of the physical phenomenon if droplet discretization in the streamwise direction is considered. Under the present restrictions the model conveys a suitable time-averaged picture over a characteristic time based on streamwise droplet spacing and droplet velocity. Once the first stream has ignited, ignition of the second stream is retarded when it is located farther from the first stream. For an overall equivalence ratio of one, ignition delays for the second stream are decreased when droplet size is decreased or when fuel volatility is increased.

REFERENCES

[1] Dwyer, H.A. and Sanders, B.R., "A Detailed Study of Burning Fuel Droplets," paper No. 86-40 presented at the WSS/CI, Banff, Canada (1986).

[2] Patnaik, G., Sirignano, W.A., Dwyer, H.A., and Sanders, B.R., "A Numerical Technique for the Solution of Vaporizing Fuel Droplets", paper presented at the 10th ICDERS, Berkeley (1985).

[3] Prakash, S. and Sirignano, W.A., "Theory of Convective Droplet Vaporization with Unsteady Heat and Mass Transfer", Intnl. J. Heat Mass Transfer, 23, 253 (1980).

[4] Labowski, M., "Calculation of the Burning Rates of Interacting Fuel Droplets", Combust. Sci. and Tech., 22, 217 (1980).

[5] Labowski, M. and Rosner, D.E., "Group Combustion of Droplets in Fuel Clouds. I: Quasi-steady Predictions", Advances in Chemistry Series, No. 166 Evaporation-Combustion of Fuels (J.T. Zung Ed.) American Chemical Society (1978).

[6] Twardus, E.M. and Brzustowski, T.A., "The Interaction Between Two Burning Fuel Droplets", Archiwum Processor Spalanio, 8, 347 (1977).

[7] Aggarwal, S.K. and Sirignano, W.A., "Unsteady Spray Flame Propagation in a Closed Volume", Combust. Flame, 62, 1, 69 (1985).

[8] Aggarwal, S.K. and Sirignano, W.A., "Ignition of Fuel Sprays: Deterministic Calculations for Idealized Droplet Arrays", Combustion, The Combustion Institute, 1773 (1985).

[9] Seth, B., Aggarwal, S.K., and Sirignano, W.A., "Flame Propagation Through an Air-Fuel Spray Mixture with Transient Droplet Vaporization", Combust. Flame, 39, 149 (1980).

[10] Sangiovanni, J.J. and Kesten, A.S., "Effect of Droplet Interaction on Ignition in Monodispersed Droplet Streams", Sixteenth Symposium (Int'l.) on Combustion, The Combustion Institute, 677 (1977).

[11] Ashgriz, N. and Yao, S.C., "Mechanism of Flame Propagation in a Spray", Paper No. 70, Fall Technical Meeting of the Eastern States Section of the Combustion Institute (1984).

[12] Rangel, R.H. and Sirignano, W.A., "Rapid Vaporization and Heating of Two Parallel Fuel Droplet Streams", to appear in Twenty First Symposium (Int'l) on Combustion, The Combustion Institute (1987).

[13] Westbrook, C.K, and Dryer, F.L., "Chemical Kinetic Modeling of Hydrocarbon Combustion", Prog. Energy Combust. Sci., 10, 1 (1984).

[14] Tong, A.Y. and Sirignano, W.A., "Analytical Solution for Diffusion and Circulation in a Vaporizing Droplet", Nineteenth Symposium (Int'l) on Combustion, The Combustion Institute, 1007 (1983).

[15] Sirignano, W.A., "Theory of Multicomponent Fuel Droplet Vaporization", presented at the V Intnl. Symposium on Combustion Processes, Poland, p. 12 [1977).

[16] Law, C.K., "Unsteady Droplet Combustion with Droplet Heating", Combust. Flame, 26, 17 (1976).

[17] Roach, G.F., "Green's Functions", 2nd Ed., Cambridge University Press, Cambridge (1982).

[18] Carslaw, H.S., and Jaeger, J.C., "Conduction of Heat in Solids", Clarendon Press, London (1959).

[19] Ozisik, M.N., "Boundary Value Problems of Heat Conduction", International Textbook Company, Scranton, PA (1968).

Table 1.
Droplet Vaporization Distances, Lifetimes, Ignition Delays, and Flame Propagation Rates for Different Stream Arrangements

Stream Arrangement		A	B	C
droplet vaporization distance (cm)	I	31	30	30
	II	33	38	45
droplet lifetimes (ms)	I	43	42	42
	II	48	57	70
ignition delay (ms)		3	15	25
transverse flame-propagation rate (cm/s)		34	13	12

Table 2.
Droplet Vaporization Distances, Lifetimes, Ignition Delays, and Flame Propagation Rates for Different Fuels and Different Inlet Droplet Diameters

Fuel		n-decane		n-hexane	
inlet diameter (μm)		100	50	100	50
droplet vaporization distance (cm)	I	30	9	20	7
	II	38	13	26	9
droplet lifetime (ms)	I	42	14	28	9
	II	57	20	37	13
ignition delay (ms)		15	6	11	4
transverse flame-propagation rate (cm/s)		13	34	19	47

FIGURE CAPTIONS

1. Schematic of the problem and coordinate system.

2. Gas-phase temperature profiles at different streamwise locations. Fuel: n-decane, Droplet Diameter: 100 μm.

3. Gas-phase fuel mass fraction contours. Fuel: n-decane, Droplet Diameter: 100 μm.

4. Gas-phase oxygen mass fraction profiles at different streamwise locations. Fuel: n-decane, Droplet Diameter: 100 μm.

5. Reaction rate profile at streamwise location ζ = 0.32.

6. Reaction rate profile at streamwise location ζ = 0.49.

7. Reaction rate profile at streamwise location ζ = 0.58.

8. Reaction rate profile at streamwise location ζ = 0.70.

9. Droplet temperature vs. downstream distance. I: left stream, II: right stream. Fuel: n-decane, Droplet Diameter: 100 μm.

10. Droplet vaporization-rate vs. downstream distance. I: left stream, II: right stream. Fuel: n-decane, Droplet Diameter: 100 μm.

11. Effective mass transfer number vs. downstream distance. I: left stream, II: right stream. Fuel: n-decane, Droplet Diameter: 100 μm.

12. Droplet radius squared vs. downstream distance. I: left stream, II: right stream. Fuel: n-decane, Droplet Diameter: 100 μm.

13. Gas-phase fuel mass fraction contours for stream arrangement A. Fuel: n-decane, Droplet Diameter: 100 μm.

14. Gas-phase fuel mass fraction contours for stream arrangement C. Fuel: n-decane, Droplet Diameter: 100 μm.

15. Droplet radius squared vs. downstream distance. I: left stream, II: right stream, Fuel: n-decane, Droplet Diameter: 50 μm.

16. Gas-phase fuel mass fraction contours. Fuel: n-decane, Droplet Diameter: 50 μm.

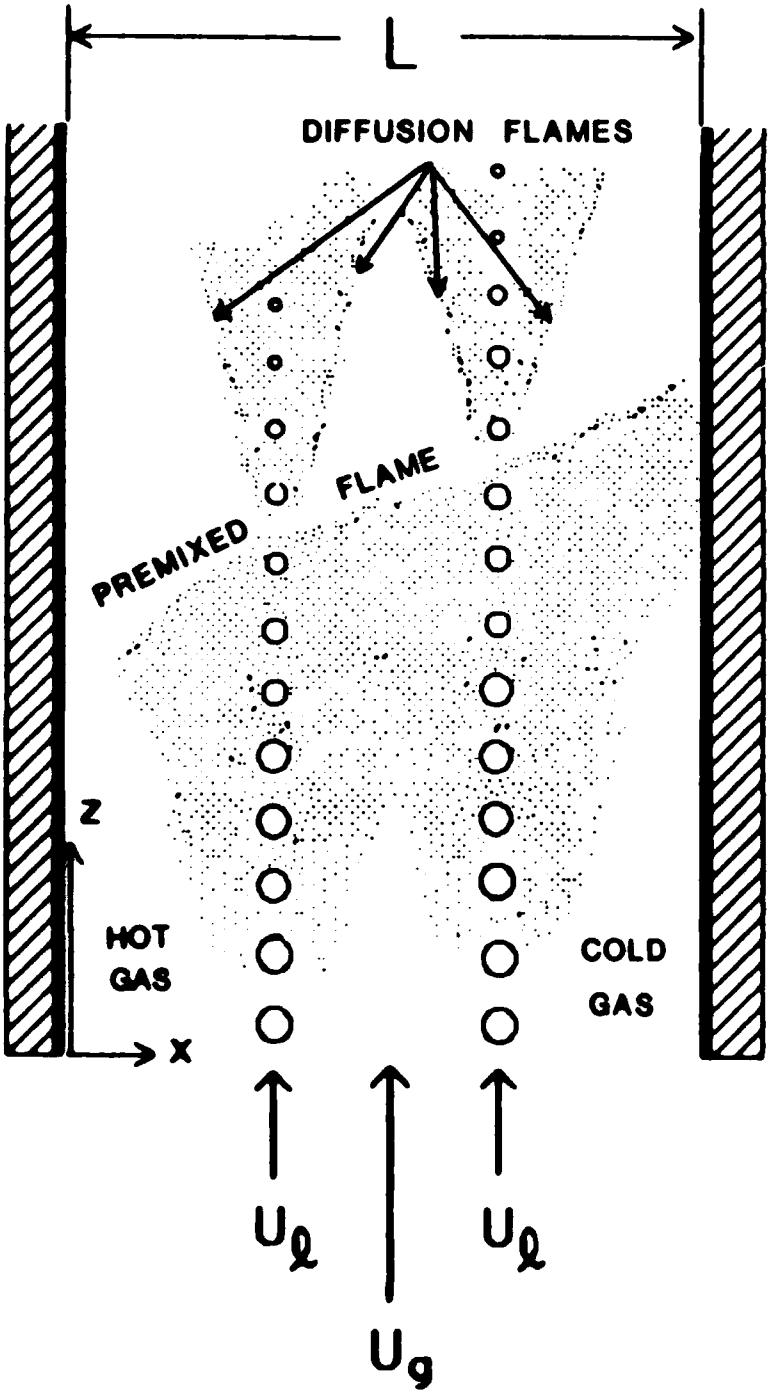
L
DIFFUSION FLAMES
PREMIXED
FLAME
Z
HOT
GAS
X
COLD
GAS
U_ℓ
U_ℓ
U_g

Fig. 1

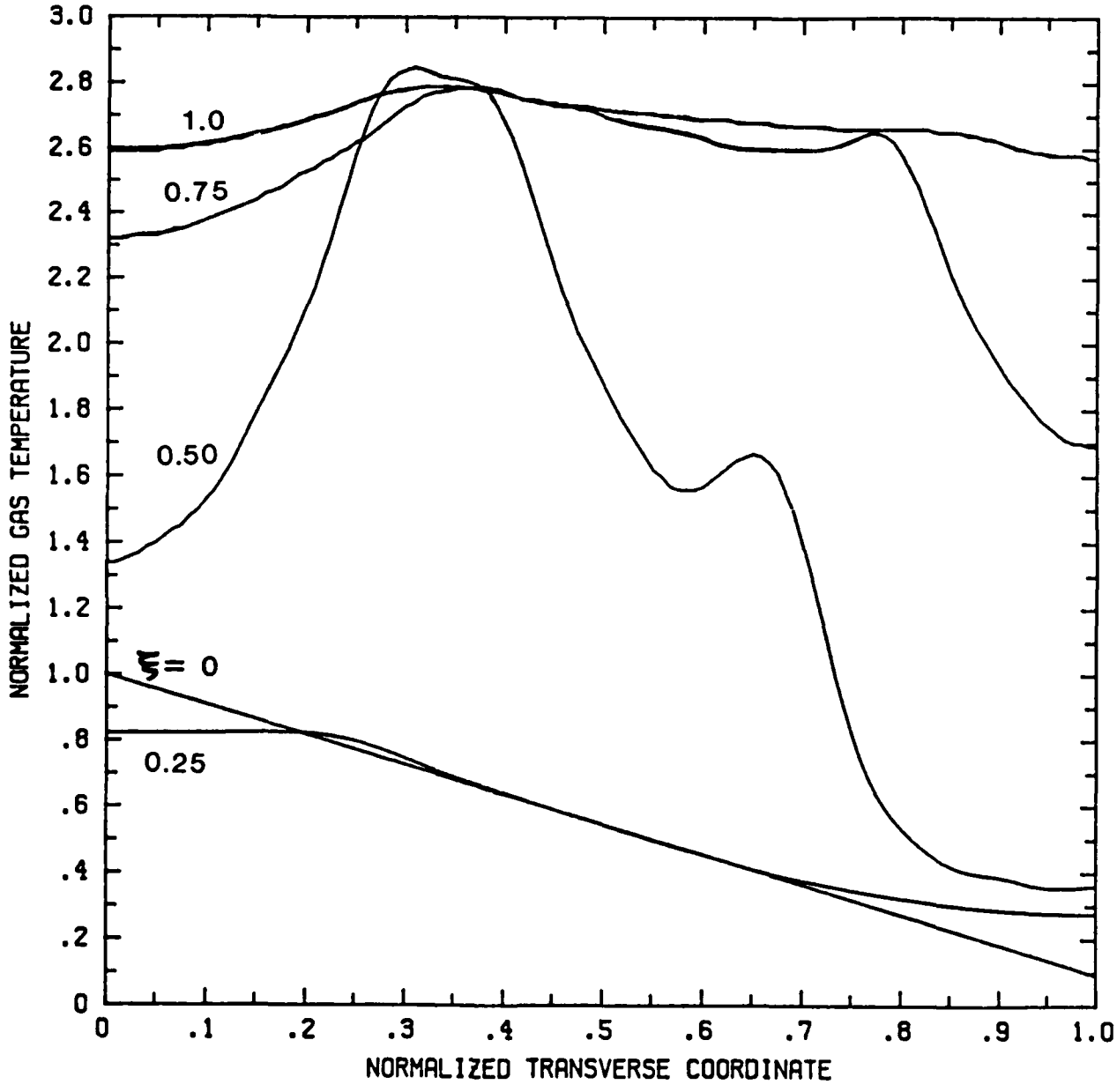
NORMALIZED GAS TEMPERATURE
NORMALIZED TRANSVERSE COORDINATE
1.0
0.75
0.50
0.25
ξ = 0
3.0
2.8
2.6
2.4
2.2
2.0
1.8
1.6
1.4
1.2
1.0
.8
.6
.4
.2
0
.1
.2
.3
.4
.5
.6
.7
.8
.9
1.0

Fig. 2

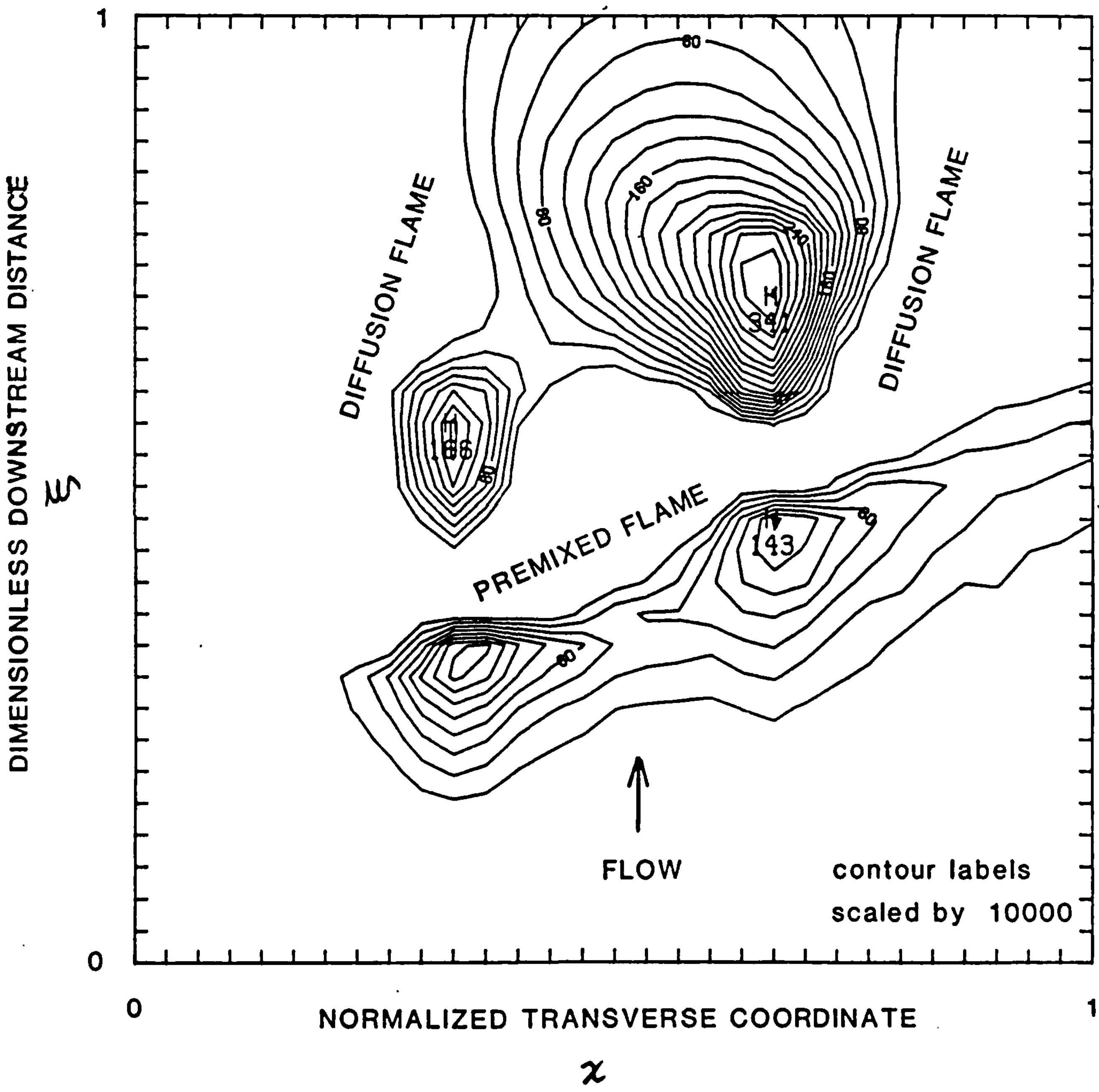

DIMENSIONLESS DOWNSTREAM DISTANCE
ξ
NORMALIZED TRANSVERSE COORDINATE
x
0
1
0
1
DIFFUSION FLAME
DIFFUSION FLAME
PREMIXED FLAME
FLOW
contour labels
scaled by 10000
H
166
H
341
H
143
80
160
240

Fig. 3

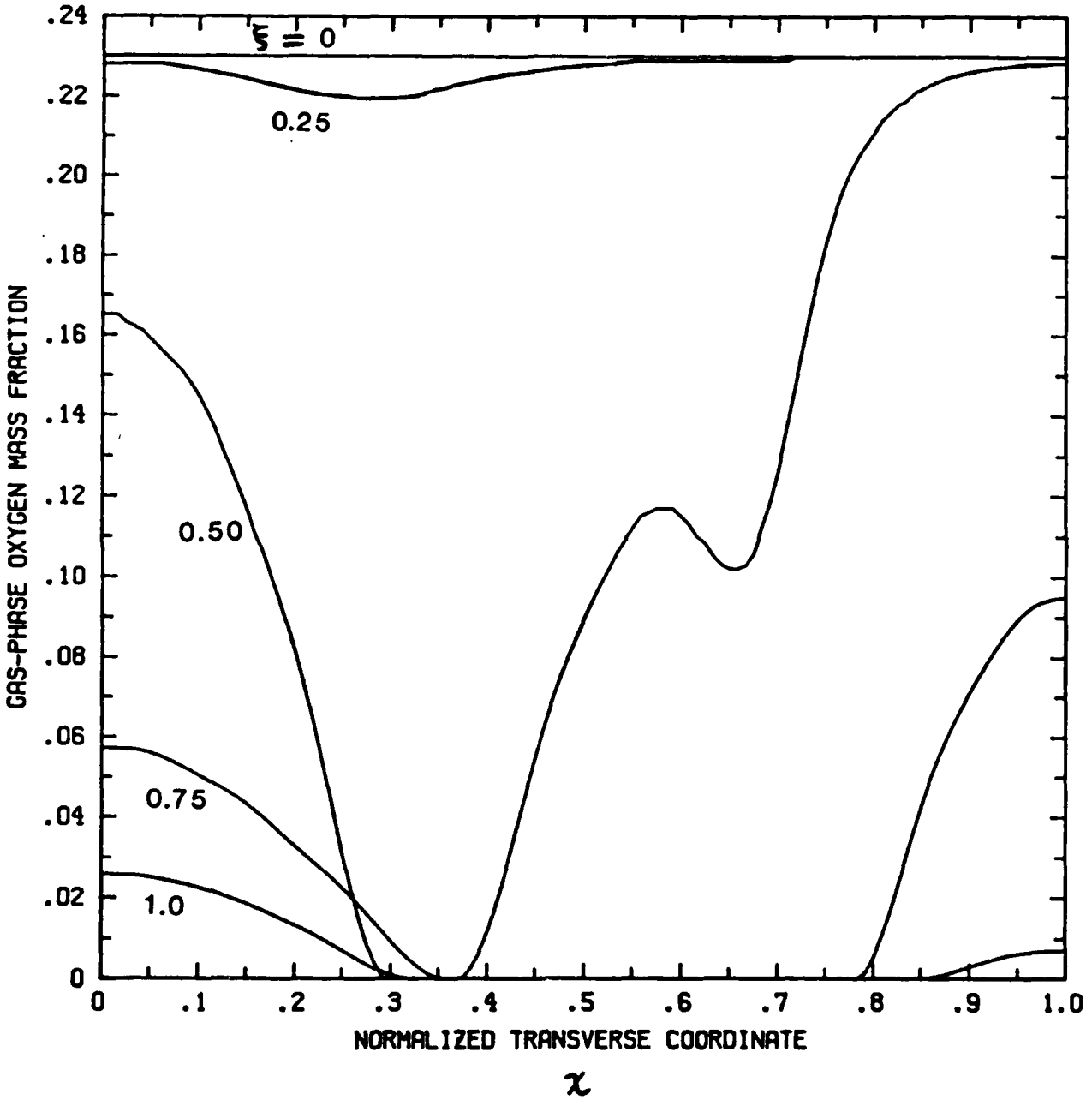
.24
.22
.20
.18
.16
.14
.12
.10
.08
.06
.04
.02
0
ξ = 0
0.25
0.50
0.75
1.0
GAS-PHASE OXYGEN MASS FRACTION
0
.1
.2
.3
.4
.5
.6
.7
.8
.9
1.0
NORMALIZED TRANSVERSE COORDINATE
χ

Fig. 4

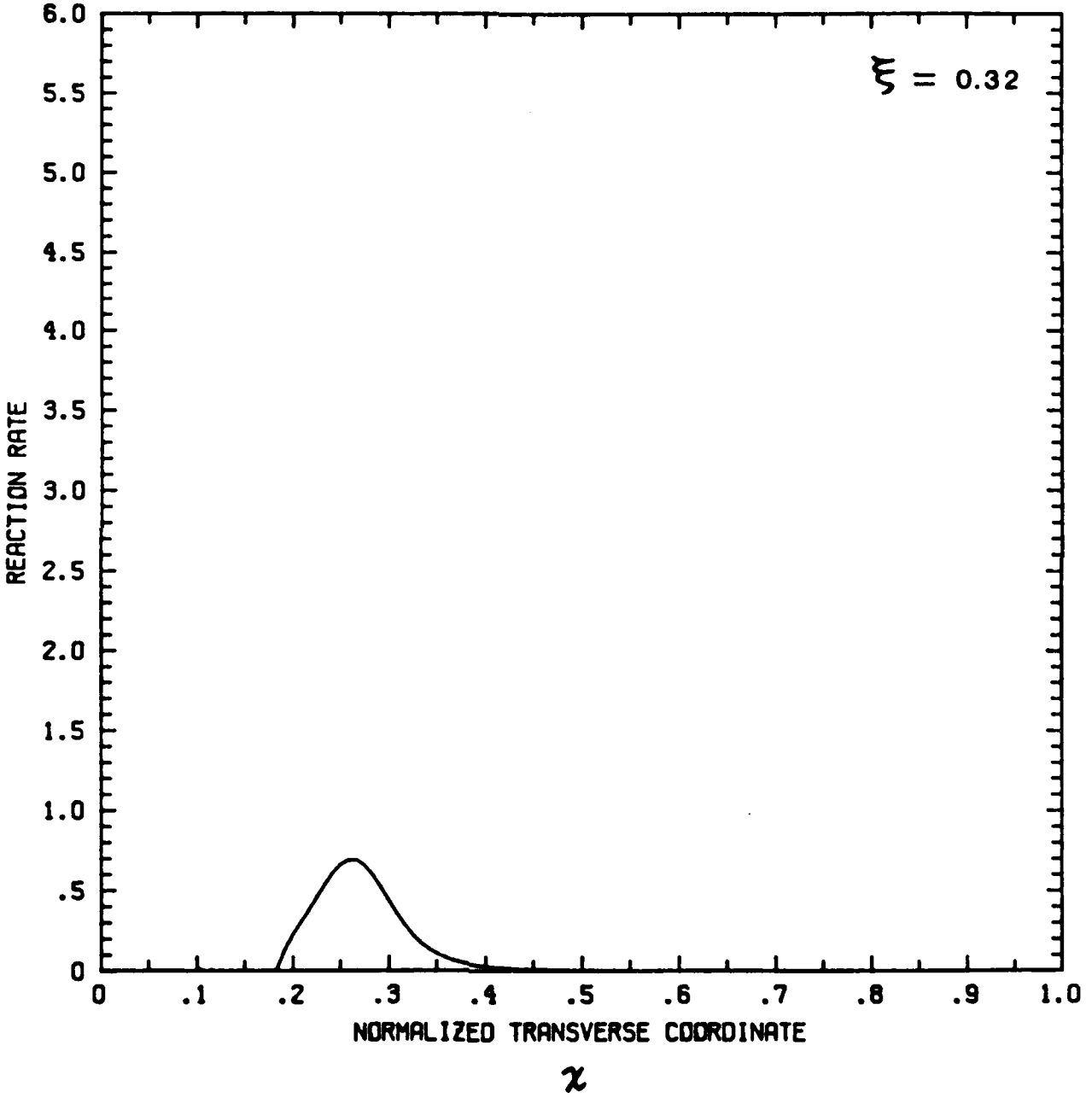
6.0
5.5
5.0
4.5
4.0
3.5
3.0
2.5
2.0
1.5
1.0
.5
0
REACTION RATE
ξ = 0.32
0
.1
.2
.3
.4
.5
.6
.7
.8
.9
1.0
NORMALIZED TRANSVERSE COORDINATE
χ

Fig. 5

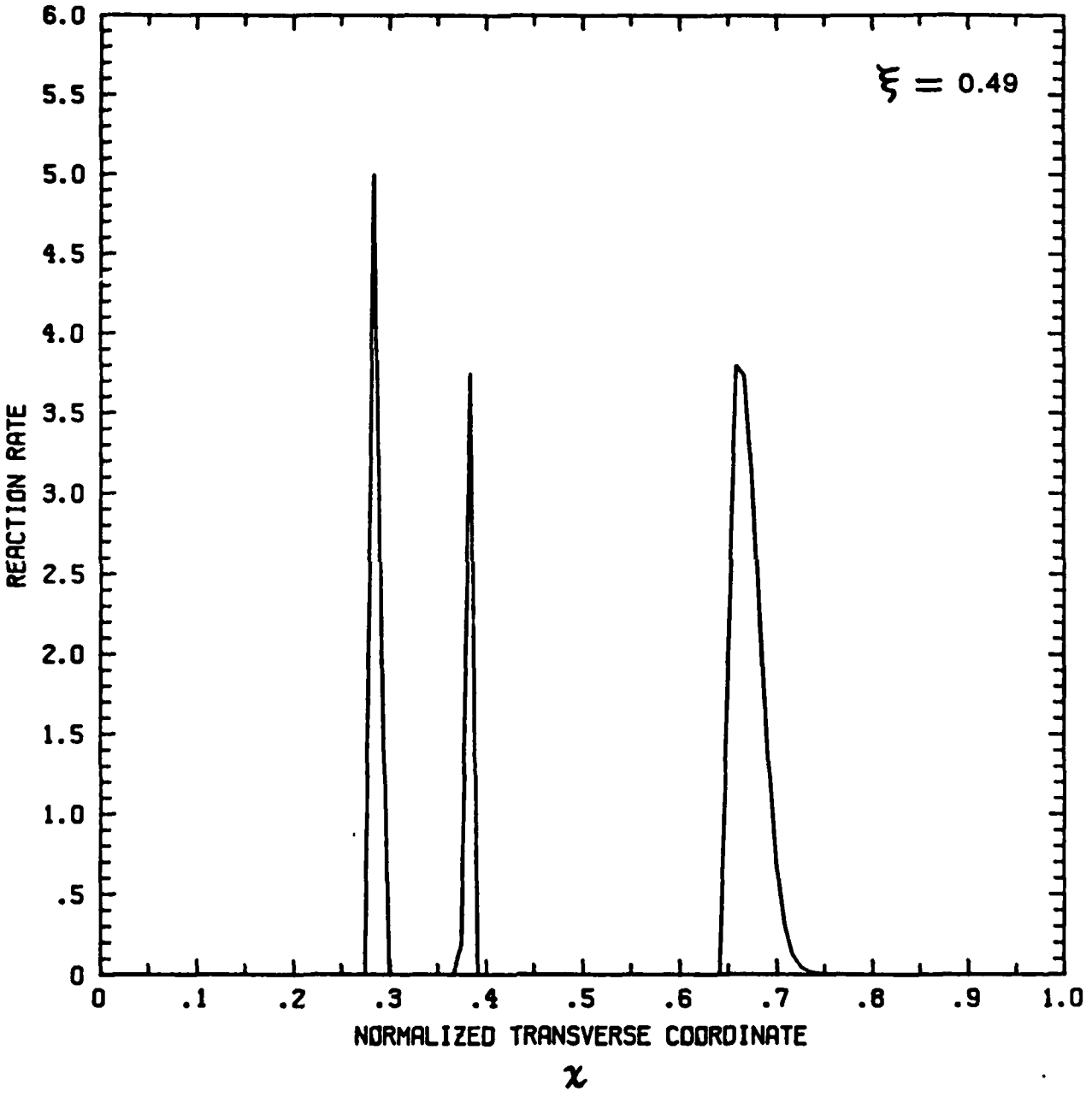
6.0
5.5
5.0
4.5
4.0
3.5
3.0
2.5
2.0
1.5
1.0
.5
0
REACTION RATE
ξ = 0.49
0
.1
.2
.3
.4
.5
.6
.7
.8
.9
1.0
NORMALIZED TRANSVERSE COORDINATE
χ

Fig. 6

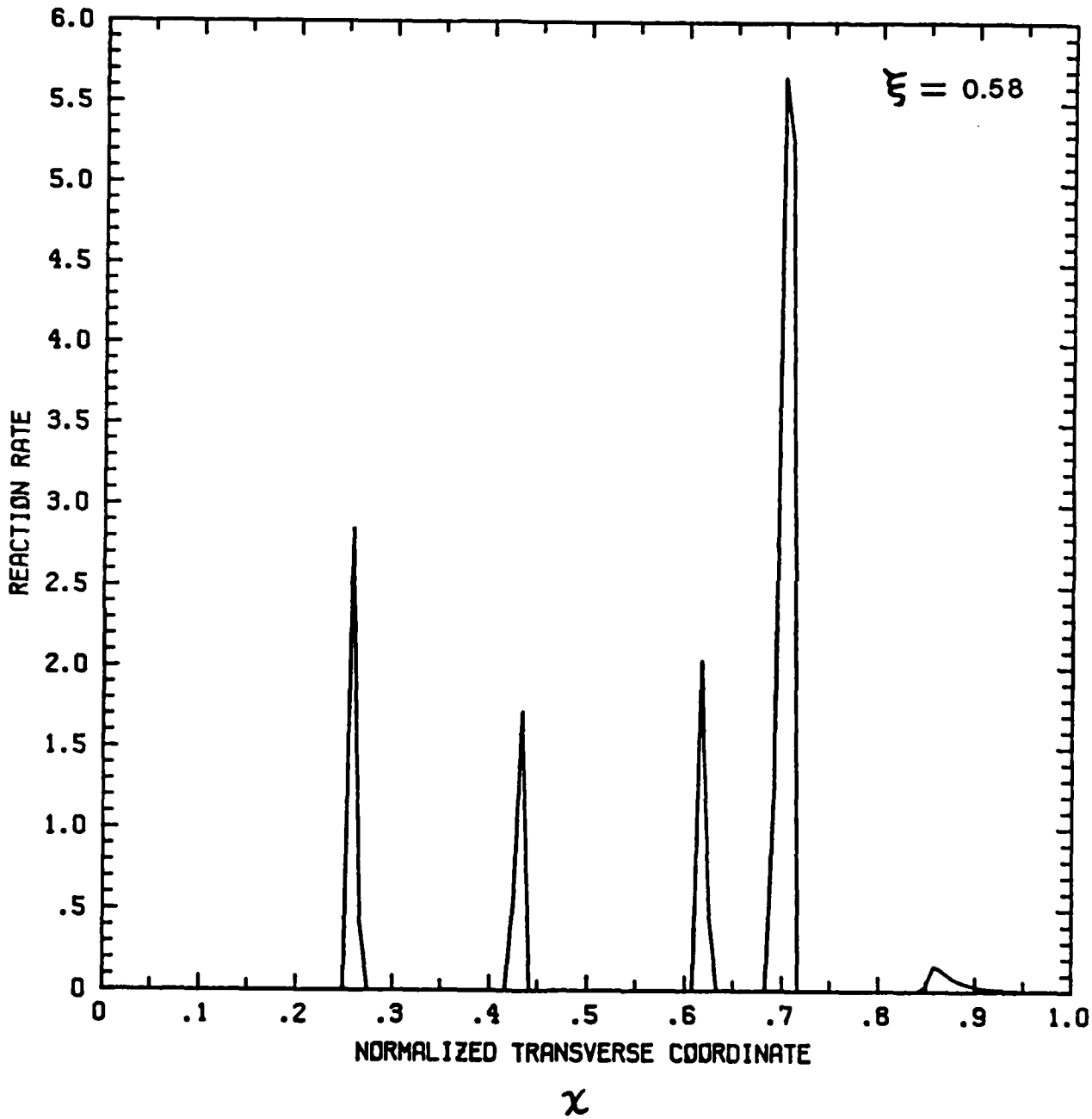
6.0
5.5
5.0
4.5
4.0
3.5
3.0
2.5
2.0
1.5
1.0
.5
0
REACTION RATE
ξ = 0.58
0
.1
.2
.3
.4
.5
.6
.7
.8
.9
1.0
NORMALIZED TRANSVERSE COORDINATE
χ

Fig. 7

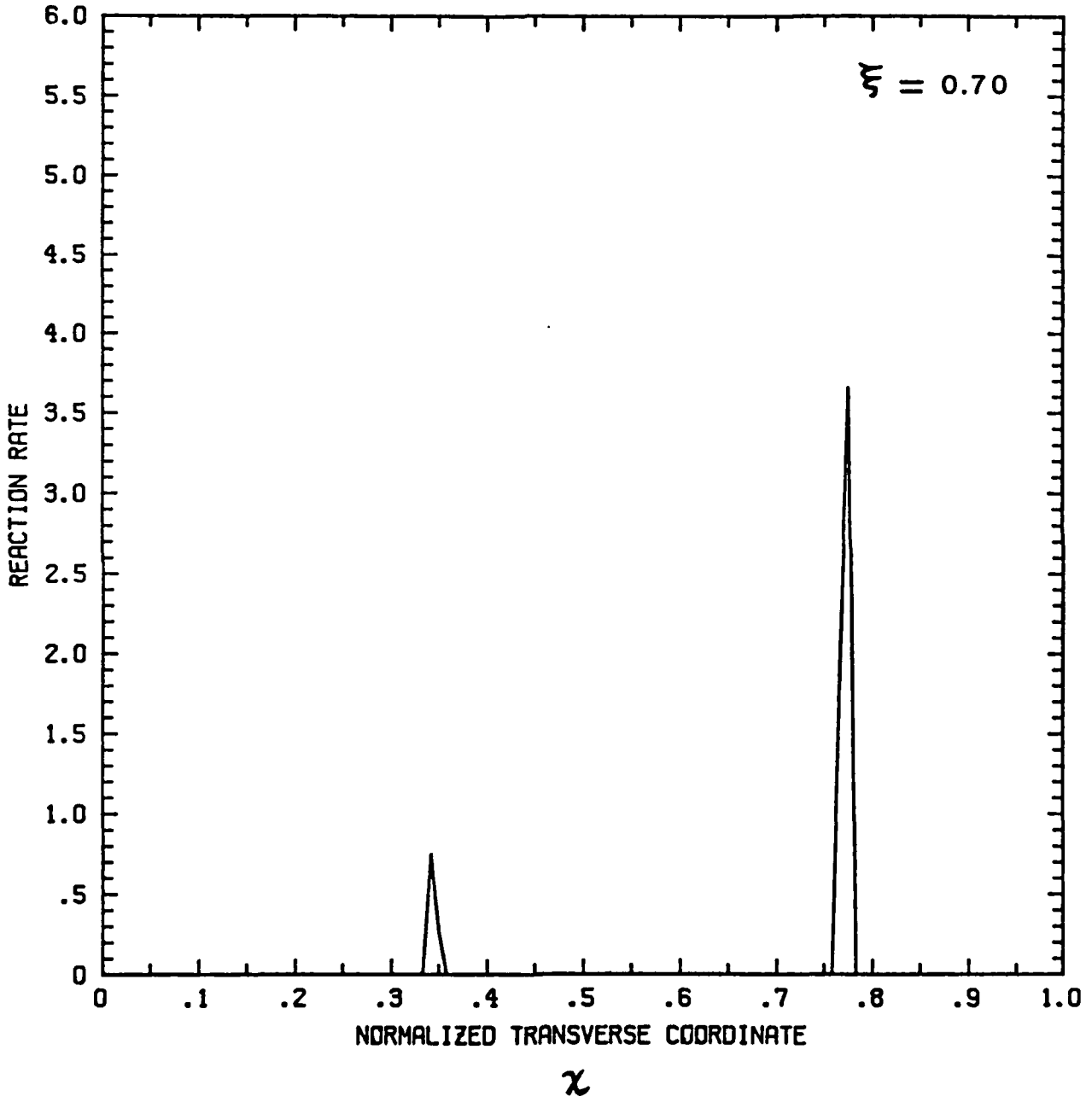
6.0
5.5
5.0
4.5
4.0
3.5
3.0
2.5
2.0
1.5
1.0
.5
0
REACTION RATE
$\xi = 0.70$
0
.1
.2
.3
.4
.5
.6
.7
.8
.9
1.0
NORMALIZED TRANSVERSE COORDINATE
χ

Fig. 8

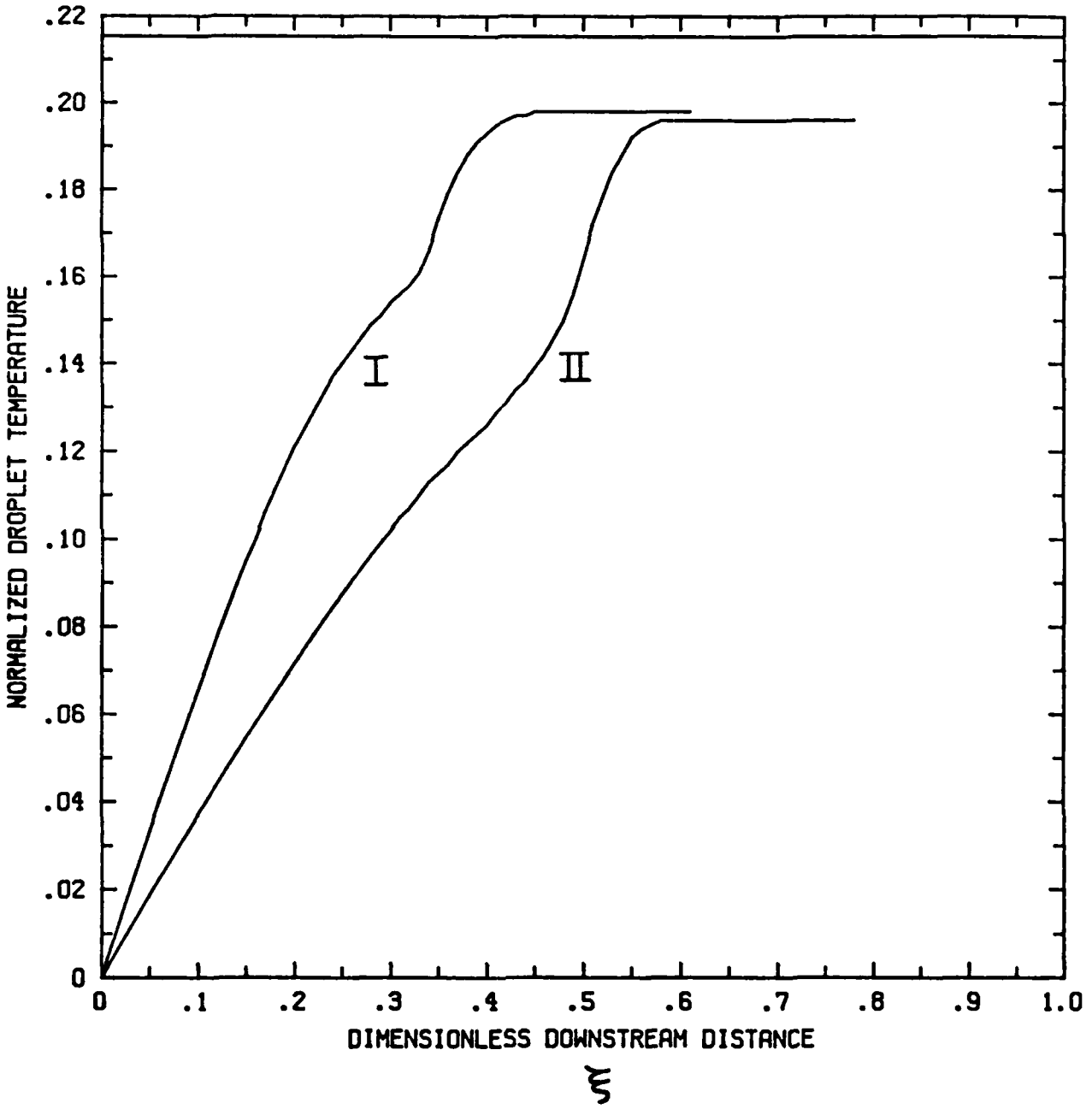
.22
.20
.18
.16
.14
.12
.10
.08
.06
.04
.02
0
NORMALIZED DROPLET TEMPERATURE
I
II
0
.1
.2
.3
.4
.5
.6
.7
.8
.9
1.0
DIMENSIONLESS DOWNSTREAM DISTANCE
ξ

Fig. 9

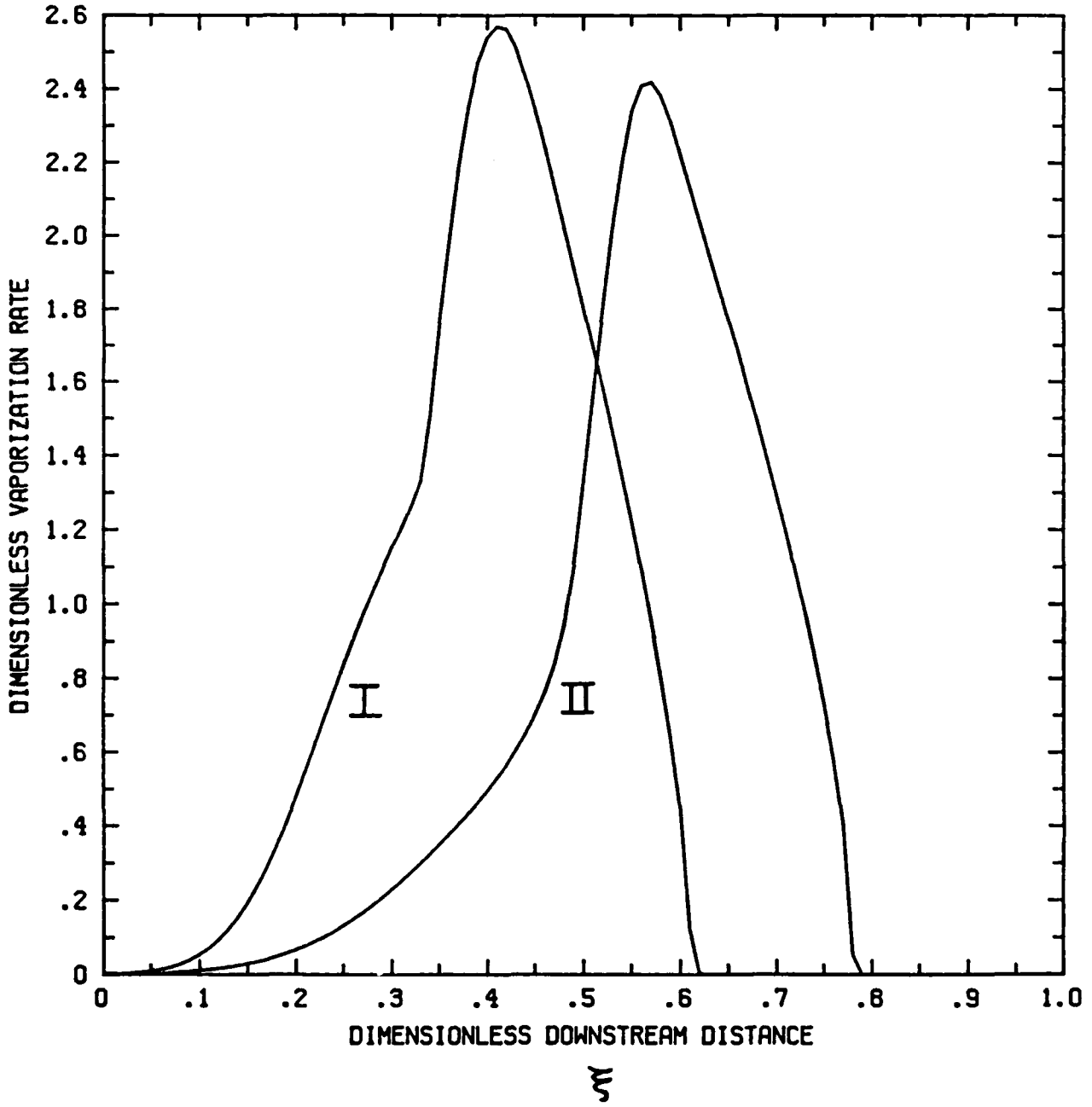
DIMENSIONLESS VAPORIZATION RATE
2.6
2.4
2.2
2.0
1.8
1.6
1.4
1.2
1.0
.8
.6
.4
.2
0
I
II
0
.1
.2
.3
.4
.5
.6
.7
.8
.9
1.0
DIMENSIONLESS DOWNSTREAM DISTANCE
ξ

Fig. 10

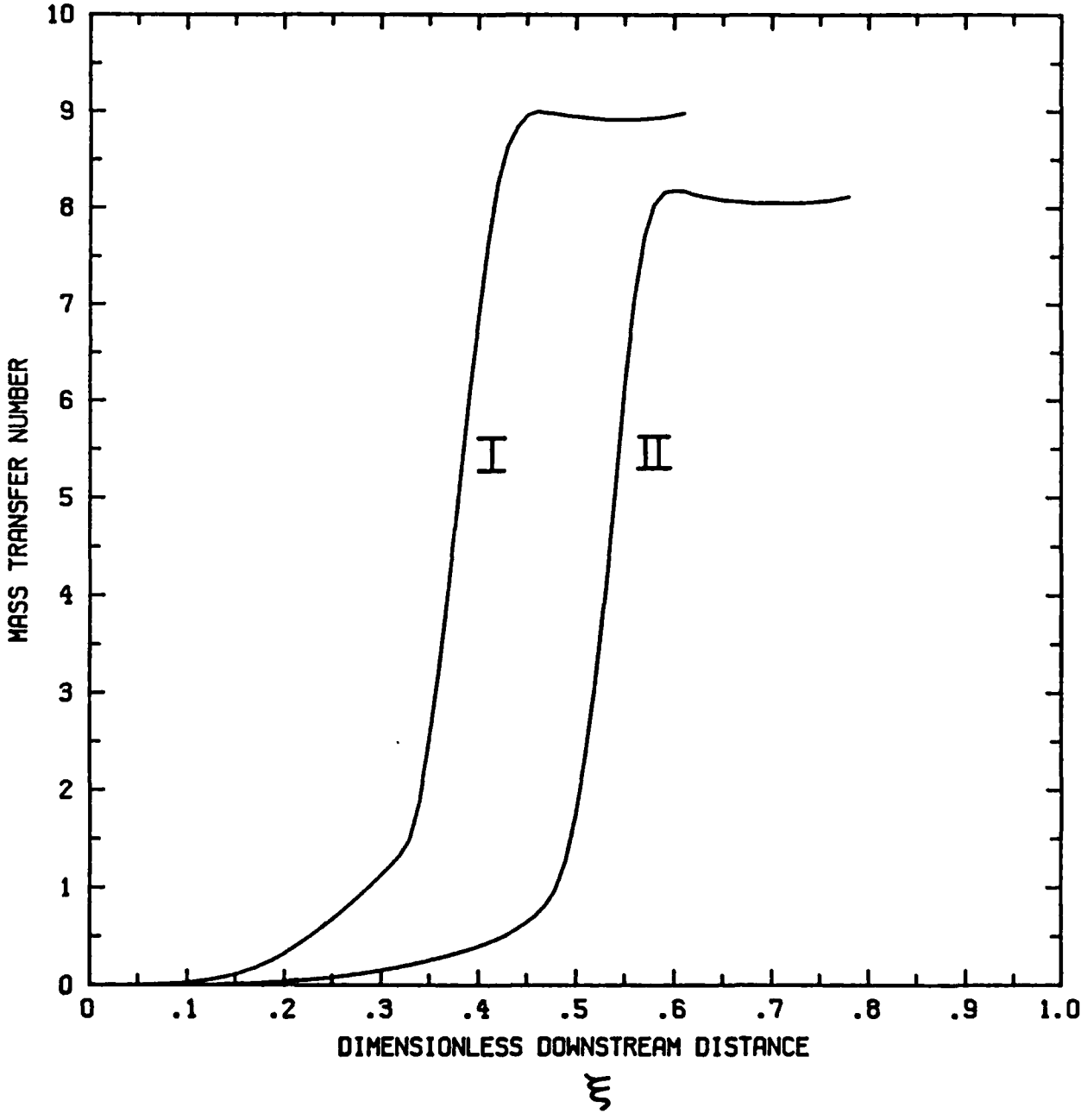
10
9
8
7
6
5
4
3
2
1
0
MASS TRANSFER NUMBER
I
II
0
.1
.2
.3
.4
.5
.6
.7
.8
.9
1.0
DIMENSIONLESS DOWNSTREAM DISTANCE
ξ

Fig. 11

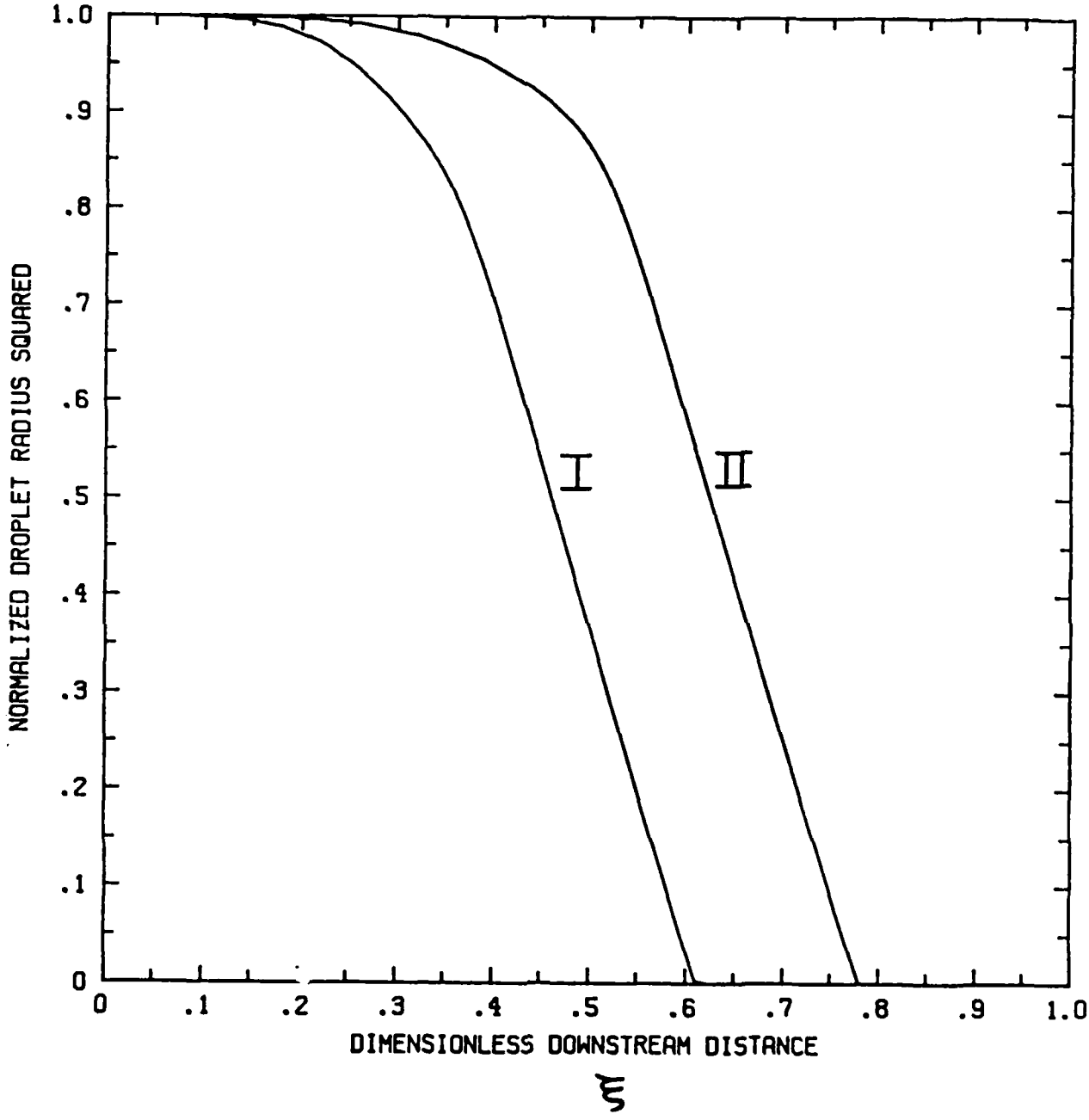
1.0
.9
.8
.7
.6
.5
.4
.3
.2
.1
0
NORMALIZED DROPLET RADIUS SQUARED
I
II
0
.1
.2
.3
.4
.5
.6
.7
.8
.9
1.0
DIMENSIONLESS DOWNSTREAM DISTANCE
ξ

Fig. 12

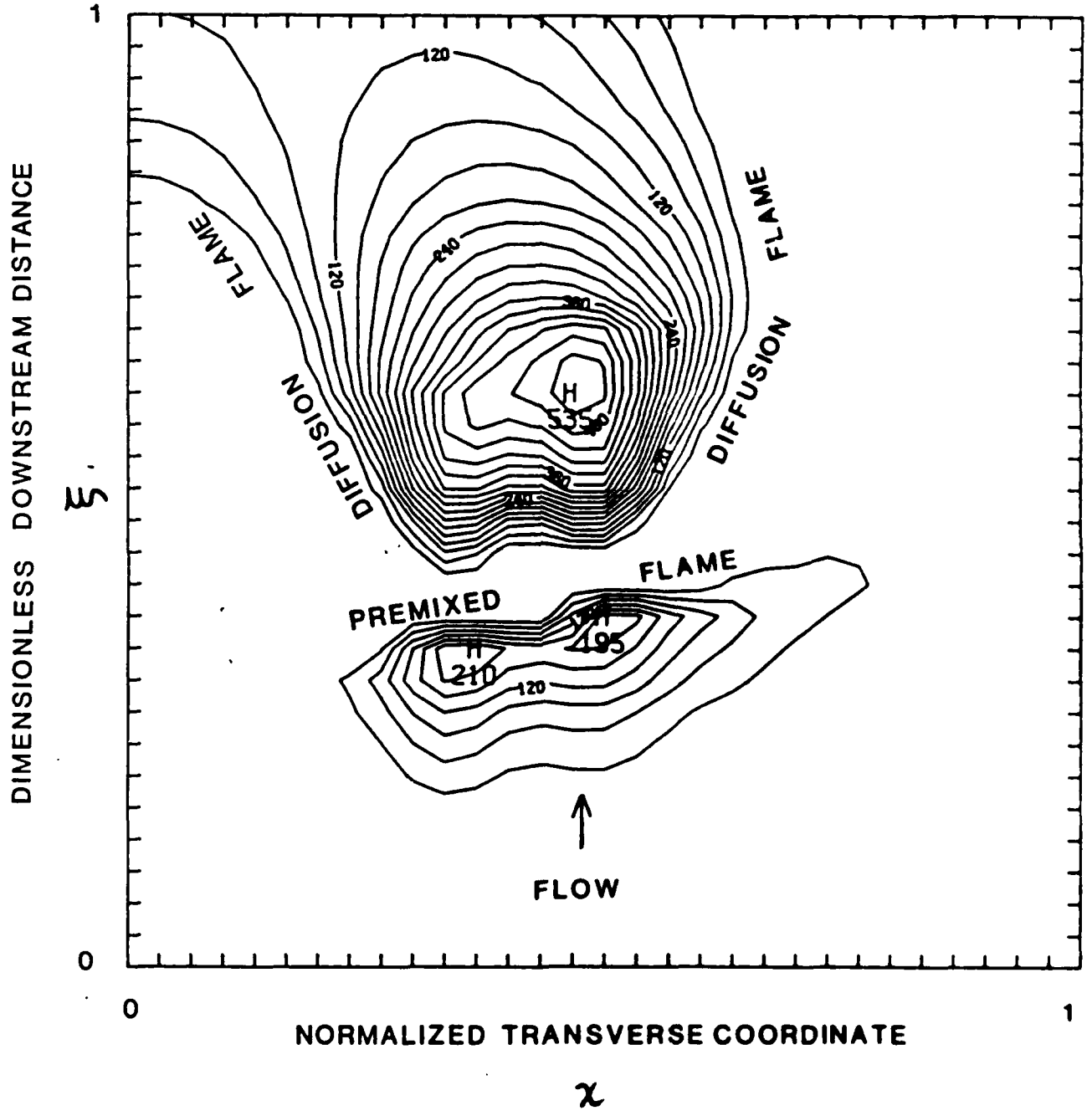
1
0
0
1
DIMENSIONLESS DOWNSTREAM DISTANCE
ξ
NORMALIZED TRANSVERSE COORDINATE
χ
FLAME
DIFFUSION
DIFFUSION FLAME
PREMIXED FLAME
FLOW
H
535
495
210
120
240
360

Fig. 13

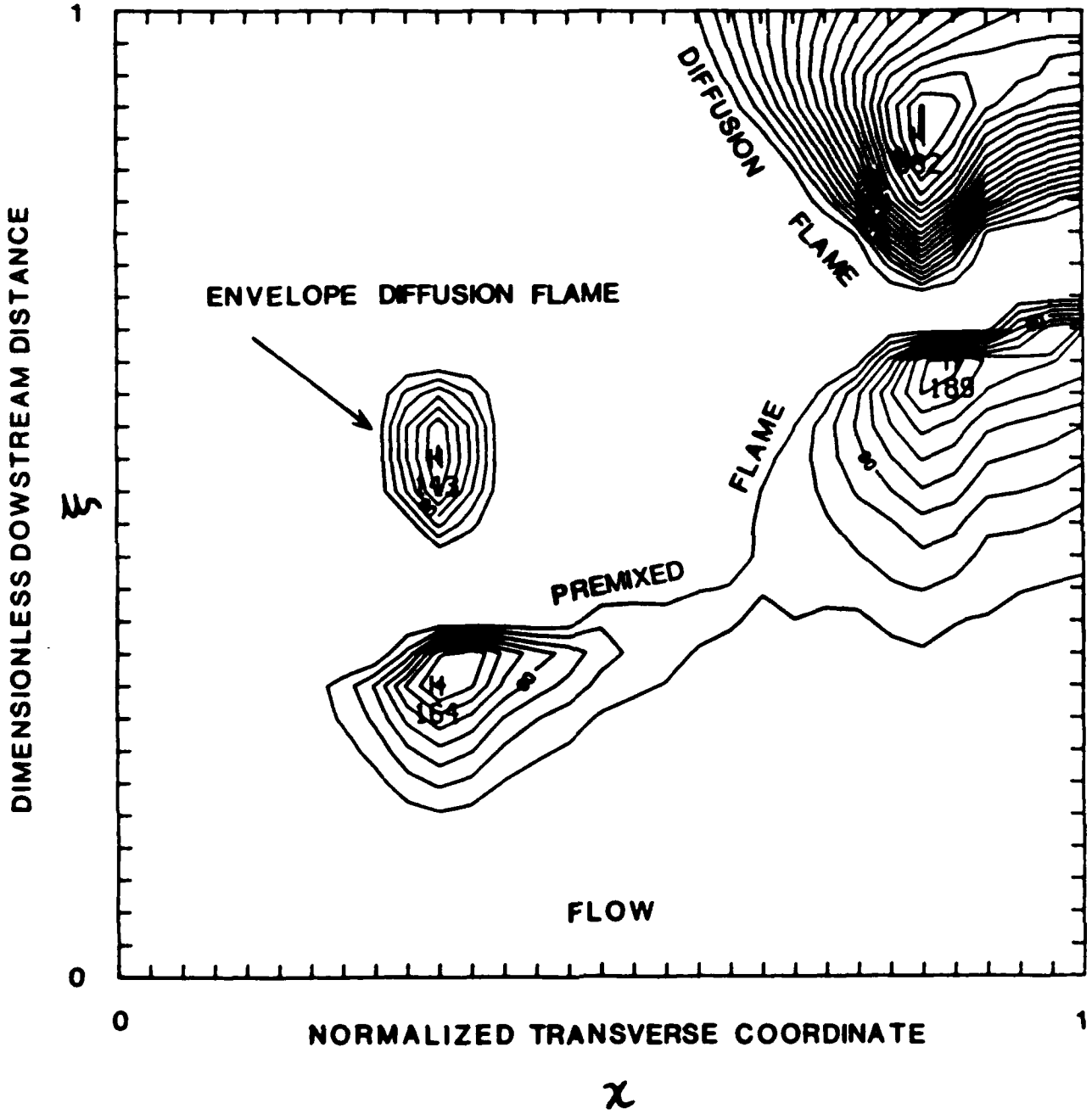
1
0
0
1
DIMENSIONLESS DOWNSTREAM DISTANCE
NORMALIZED TRANSVERSE COORDINATE
DIFFUSION FLAME
ENVELOPE DIFFUSION FLAME
FLAME
PREMIXED
FLOW

Fig. 14

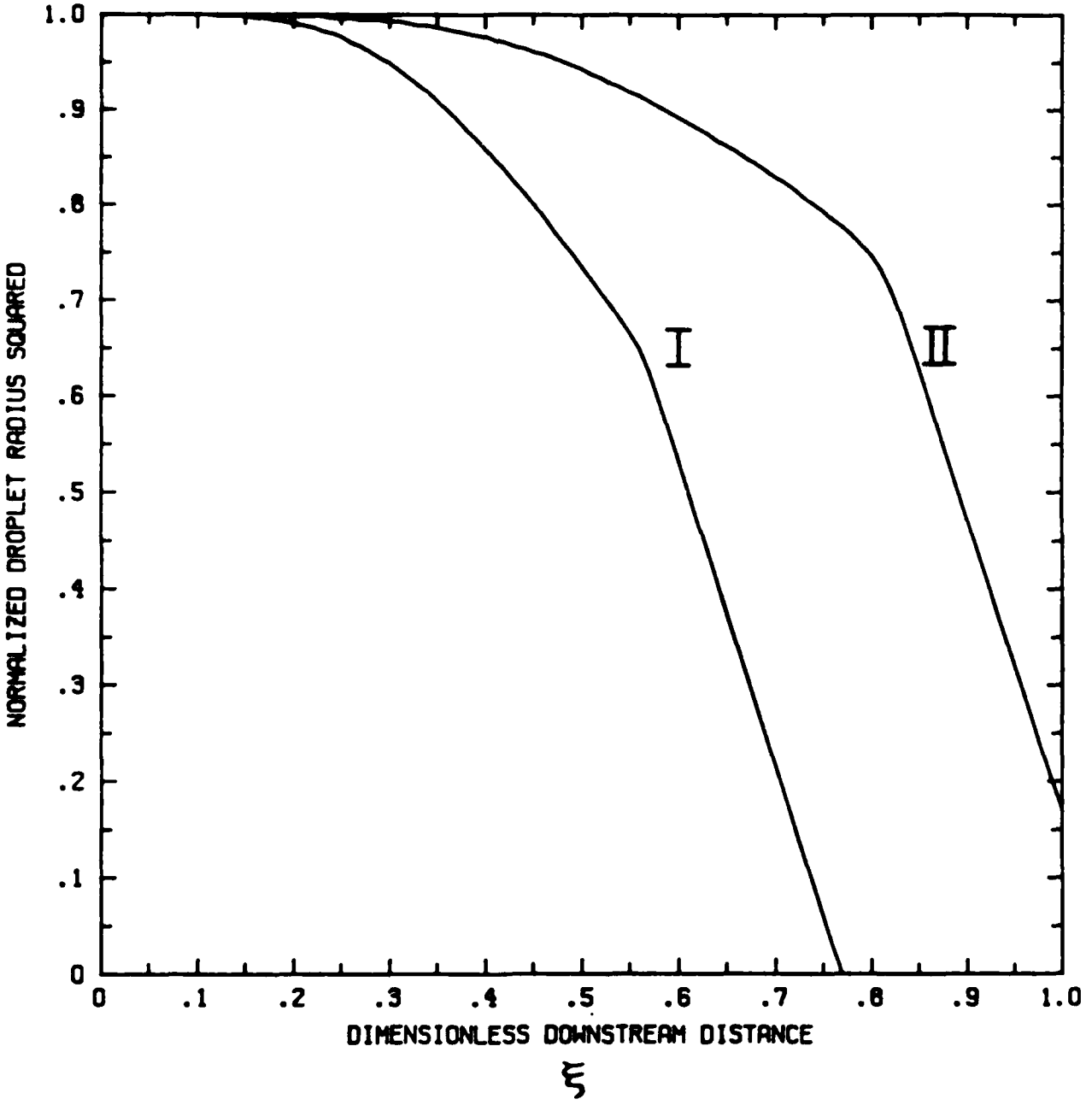
1.0
.9
.8
.7
.6
.5
.4
.3
.2
.1
0
NORMALIZED DROPLET RADIUS SQUARED
I
II
0
.1
.2
.3
.4
.5
.6
.7
.8
.9
1.0
DIMENSIONLESS DOWNSTREAM DISTANCE
ξ

Fig. 15

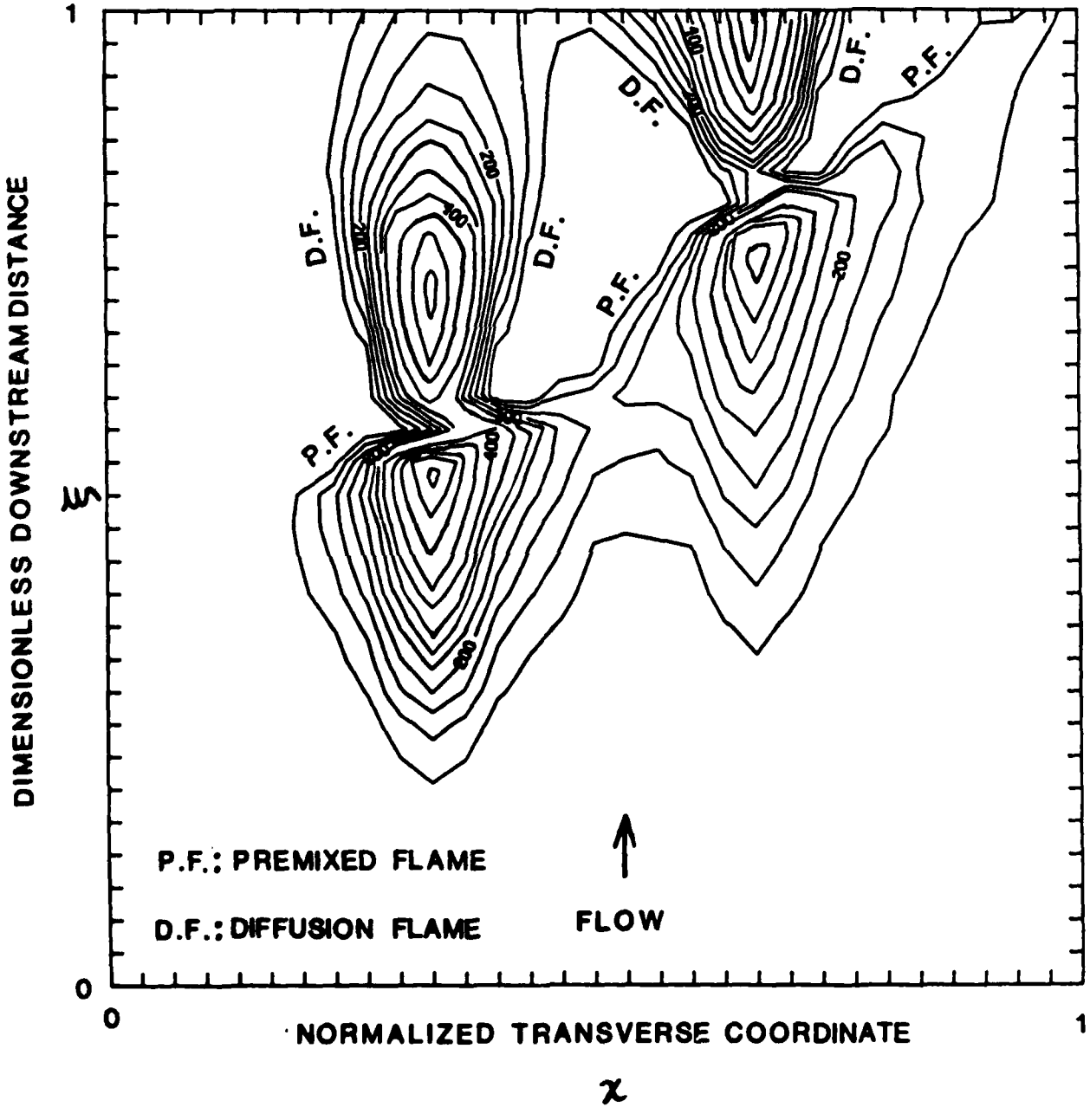

Fig. 16

END

7-87

DTIC